Current transport mechanisms in lattice-matched Pt/Au-InAlN/GaN Schottky diodes

Jian Ren, Dawei Yan,[a] Guofeng Yang, Fuxue Wang, Shaoqing Xiao, and Xiaofeng Gu
Key Laboratory of Advanced Process Control for Light Industry (Ministry of Education), Department of Electronic Engineering, Jiangnan University, Wuxi 214122, China

(Received 4 February 2015; accepted 2 April 2015; published online 15 April 2015)

Lattice-matched Pt/Au-$In_{0.17}Al_{0.83}N$/GaN hetreojunction Schottky diodes with circular planar structure have been fabricated and investigated by temperature dependent electrical measurements. The forward and reverse current transport mechanisms are analyzed by fitting the experimental current-voltage characteristics of the devices with various models. The results show that (1) the forward-low-bias current is mainly due to the multiple trap-assisted tunneling, while the forward-high-bias current is governed by the thermionic emission mechanism with a significant series resistance effect; (2) the reverse leakage current under low electric fields (<6 MV/cm) is mainly carried by the Frenkel-Poole emission electrons, while at higher fields the Fowler-Nordheim tunneling mechanism dominates due to the formation of a triangular barrier. © *2015 AIP Publishing LLC*.
[http://dx.doi.org/10.1063/1.4917566]

I. INTRODUCTION

Owing to their excellent physical properties, such as large breakdown field, high electron saturation velocity, and high thermal reliability, wide bandgap III-nitride semiconductors are extremely attractive for power electronic applications from power conditioning to microwave communication.[1,2] Thanks to the strong piezoelectric effect and the natural spontaneous polarization effect, AlGaN/GaN heterojunction high electron mobility transistors (HEMT) can output higher power density than conventional GaAs MESFET and Si LD-MOSFET, making high-efficiency and power-saving power amplification possible. Unfortunately, there exists a "critical voltage" beyond which the gate leakage current of AlGaN/GaN HEMTs begins to degrade.[3,4] Such degradation is commonly attributed to the generation of new structural defects in the AlGaN barrier layer, which suffers from a severe inverse piezoelectric effect.[5] High leakage current induced by additional defects will severely degrade the device reliability, therefore the inverse piezoelectric effect in the device should be suppressed. Currently, the lattice-matched $In_{0.17}Al_{0.83}N$/GaN heterostructure seems the most promising, which could provide higher two-dimensional electron gas (2DEG) concentration without strain and cracks offering potential reliability benefits.[6] The absence of strain allows low sheet resistances and high transconductance with high current density, making them better candidates for power electronic applications. Unfortunately, the practical $In_{0.17}Al_{0.83}N$/GaN HEMTs usually suffer from much larger gate leakage current than theoretical expectation under both the forward and reverse bias conditions, and so far the charge transport mechanisms still remain unclear. So, understanding the detailed gate leakage current transport processes is very important for improving the reliability of HEMTs.

In this paper, circular Schottky diode structures having equivalent structure and characteristics to lattice-matched InAlN/GaN HEMTs are fabricated. Their forward and reverse current transport mechanisms are investigated by performing temperature dependent current-voltage (*T-I-V*) measurements. Various models, including thermionic-emission (TE), trap-assisted tunneling (TAT), Frenkel-Poole (FP) emission, and Fowler-Nordheim (FN) tunneling, are taken into account for analyzing the experimental data. The effective defect density and the FP emission barrier height in the InAlN/GaN Schottky diodes are obtained by fitting data.

II. EXPERIMENT

The lattice-matched InAlN HEMT epiwafers are grown by metal-organic chemical vapor deposition on *c*-plane sapphire substrate, including a 3 μm i-GaN layer, a 2 nm AlN spacer, and an 18 nm i-$In_{0.17}Al_{0.83}N$ barrier layer. The 2DEG density at the InAlN/GaN interface is determined by the capacitance-voltage measurements is about $2.6 \times 10^{13}\,cm^{-2}$, quite close to the result obtained from the Hall measurements. The schematic cross-section and the top-view optical micrograph of the fabricated InAlN/GaN hetreojunction Schottky diode are shown in Fig. 1. The electrode structure consists of circular Schottky dots of 100 μm in diameter separated radially by 10 μm from the Ohmic metals. The standard lithography and lift-off technique are used to pattern the Pt/Au-based Schottky contact dots. Ohmic contact are formed by annealing a Ti/Al/Ni/Au metal stack using rapid thermal annealing in N_2 at 870 °C for about 30 s. Two 100×100 μm^2 pads are deposited to obtain reliable contacts between the test probe and underlying electrodes. Finally, a 150-nm-thick silicon nitride film is deposited on the sample surface as the passivation layer. Temperature dependent *I-V* characteristics of the diodes are measured using a Keithley 4200 SCS semiconductor parameter analyzer and a MAC3C SHIMAX digital temperature controller.

[a]E-mail: daweiyan@jiangnan.edu.cn

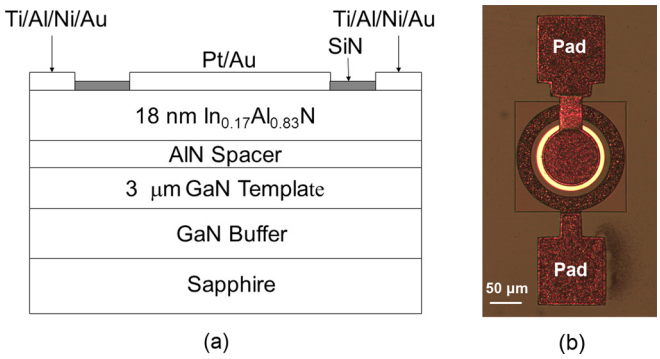

FIG. 1. Schematic cross-section (a) and top-view optical micrograph (b) of the fabricated Pt/Au-InAlN/GaN Schottky diode.

III. RESULTS AND DISCUSSION

Figure 2 shows typical *I-V* characteristics of the InAlN/GaN Schottky diodes measured from 300 K to 500 K with a step of 50 K. It is found that (1) at forward bias lower than 2 V, the current increases exponentially with the applied bias, while at higher bias the current increases slowly due to the significant series resistance effect; (2) the increasing rate of leakage current gradually decreases with the reverse bias; and (3) the reverse current at low bias shows a stronger temperature dependence than that at high reverse bias. Based on these features, next we will discuss the charge transport mechanisms of the InAlN/GaN Schottky diode at forward and reverse directions by considering various transport models.

A. Forward current transport mechanism

The current characteristics of conventional ideal Schottky diodes are commonly described by the traditional TE model. In this model, only carriers (electrons or holes) with energy greater than the potential barrier can flow from the semiconductor into the metal freely at a certain temperature, and vice versa. In this regime, the TE current (I_{TE}) does not depend on the barrier shape and the dopant distribution, which can be expressed by[7]

$$I_{TE} = I_0 \exp\left[\frac{q(V - IR_S)}{kT}\right], \tag{1a}$$

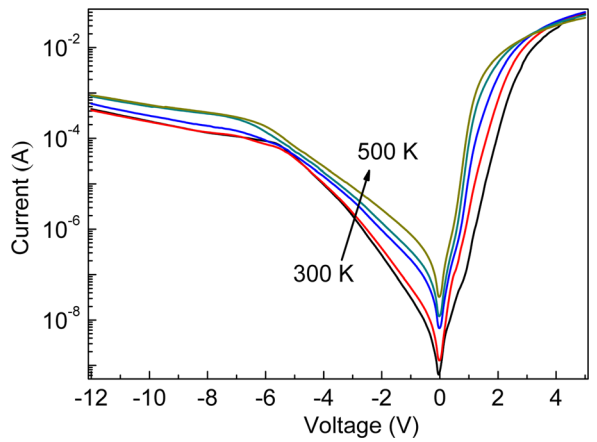

FIG. 2. Temperature dependent *I-V* characteristics of InAlN/GaN Schottky diode.

$$I_0 = AA^*T^2 \exp\left(\frac{-q\Phi_{b0}}{kT}\right), \tag{1b}$$

where I_0 is the saturation current, T is the absolute temperature, R_S is the Schottky series resistance, k is Boltzmann's constant, $A \sim 7.85 \times 10^{-5}$ cm^2 is the effective contact area, A^* is the effective Richardson constant (55.7 A·cm^{-2}·K^{-2} for InAlN),[8] and $q\Phi_{b0}$ is the zero-bias Schottky barrier height. However, the forward-low-bias *I-V* data cannot be well fitted with Eq. (1a), indicating that a single TE model is not adequate to describe the current. It is worth noting that III-Nitride materials contain a large number of structural defects, which can introduce high density of deep level trap states within the bandgap of the semiconductor, and enhance the tunneling probability of electrons. Therefore, the TAT current (I_{TAT}) might have a significant contribution to the forward current, and can be described by[9]

$$I_{TAT} = I_t\left\{\exp\left[\frac{q(V - IR_S)}{E_0}\right] - 1\right\}, \tag{2a}$$

$$I_t = Aq\nu_D D \exp\left(\frac{qV_K}{E_0}\right), \tag{2b}$$

where I_t is the saturation tunneling current, $\nu_D \sim 1.5 \times 10^{13}$ s^{-1} is the Debye frequency, D is the effective defect density, qV_k is the diffusion barrier, and $E_0 = E_{00}\coth(E_{00}/kT)$ is the tunneling parameter, where E_{00} is the characteristic tunneling energy related to the tunnel effect transmission probability.[9] In addition, when the applied bias is sufficient low, the edge leakage current (I_{RL}) could become dominant, given by

$$I_{RL} = \frac{V - IR_s}{R_{sh}}, \tag{3}$$

where R_{sh} is the shunt resistance, which can be determined from the reverse *I-V* curve of the device.[10]

We use the above equations to fit the forward *I-V* characteristics at different temperatures, and the typical fitting results at 300 K and 500 K are shown in Fig. 3. It turns out that the forward-low-bias current can be nicely described by the TAT model and the forward-high-bias current agrees well with the traditional TE mechanism, and the edge leakage current dominates at extremely low bias. Figure 4 illustrates the schematic forward transport processes of electrons: at low bias, the current is a diagonal multistep tunneling current via intermediate states distributed in the band gap of the semiconductor;[11] while at higher bias, the current is mainly carried by the TE electrons from the semiconductor into the metal.

Figure 5 shows Schottky barrier height as a function of temperature obtained from the fitting method. The barrier height is about 2.91 eV at room temperature, which decreases monotonously to 2.88 eV at elevated temperature up to 500 K, showing a small negative temperature coefficient. For III-V semiconductors, the metal Fermi level is usually pinned at about 1/3 energy position of the bandgap owing to the Femi-level pinning effect. Thus, when the bandgap width decreases with increasing temperature due to thermal contraction, $q\Phi_{b0}$ should decrease proportionally.

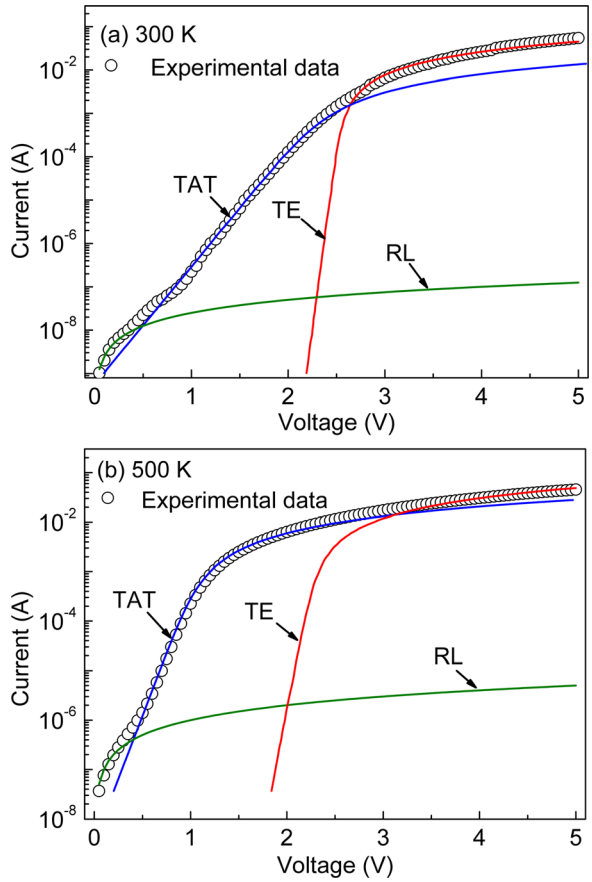

FIG. 3. Fitting results of the forward *I-V* characteristics of InAlN/GaN Schottky diode measured at 300 K (a) and 500 K (b), respectively.

Accordingly, the temperature dependence of Schottky barrier height can be written as[12]

$$q\Phi_{b0}(T) = \eta\left[E_g(0) - \frac{3.3\times10^{-4}T^2}{T+600}\right], \tag{4}$$

where η is the proportional coefficient, $E_g(0)$ ($\sim$4.7 eV) is the $In_{0.17}Al_{0.83}N$ bandgap at 0 K. As shown in Fig. 5, the derived Schottky barrier height (solid circles) can be well described with Eq. (4) with $\eta \sim 0.6$ (solid line), confirming that the negative temperature coefficient behavior is due to the thermally induced bandgap shrinkage effect. Here, the

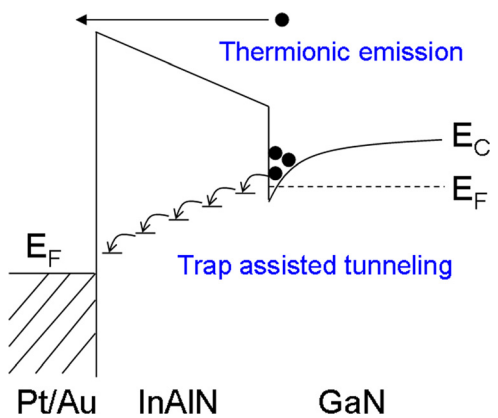

FIG. 4. Schematic diagram of the forward current transport mechanism of InAlN/GaN Schottky diode. The solid dots represent electrons in GaN.

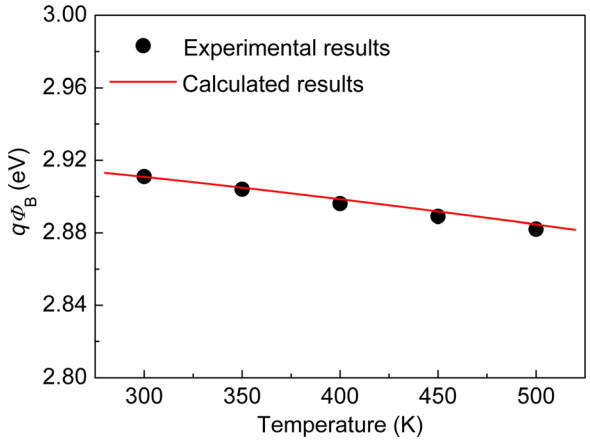

FIG. 5. Temperature dependence of the Schottky barrier height.

value of proportional coefficient is larger than the empirical value of 1/3, which can be well explained with the Fermi level depinning effect at the metal/semiconductor interface, caused by the interface states ionization at high forward injection.[13]

Figure 6 shows the temperature dependences of the tunneling saturation current I_t and tunneling parameter E_0 obtained by fitting. Clearly, I_t depends exponentially on temperature, and $E_0 \sim 0.12$ eV is almost unchanged over the temperature range from 300 K to 500 K. Rearranging Eq. (2b), the effective trap density involved in the TAT process can be calculated by

$$D = \frac{I_t(0)}{Sq\nu_D}\exp\left[\frac{qV_K(0)}{E_0}\right], \tag{5}$$

where $I_t(0)$ and $qV_K(0)$ are the values of I_t and qV_k at 0 K, respectively. Considering the bandgap shrinkage effect, $qV_K(0)$ is derived to be 2.93 eV. Extrapolating the I_t–T plot to 0 K, $I_t(0)$ is determined about 3.3×10^{-11} A. Substituting the above values into Eq. (5), the D value is determined about $5.5\times10^{9}\,cm^{-2}$. The typical bulk density of N vacancy defects in GaN materials is about 10^{16}–$10^{19}\,cm^{-3}$.[14] The corresponding surface density is determined around 10^{7}–$10^{10}\,cm^{-2}$ (assuming the lattice constant 0.5 nm). The D value falls right in this range, so we think that N vacancies

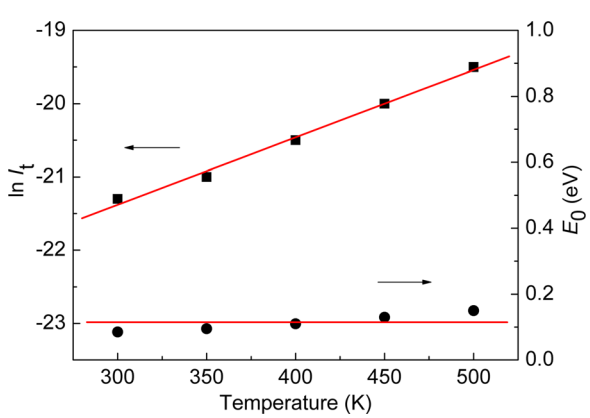

FIG. 6. Temperature dependence of the saturation tunneling current and the tunneling parameter.

might be the structural defects responsible for the TAT current.

B. Reverse current transport mechanism

Due to the strong spontaneous polarization effect, there exists a large polarization electric field in the barrier layer of InAlN/GaN heterojunctions. With respect to the polarization field, the ionized donor states at the barrier top surface and the 2DEG at the channel can generate an opposite screening electric field. As the 2DEG is gradually depleted with the external applied voltage, the net electric field will nearly linearly increase.[15] In this case, the effective emission barrier height of deep-level defect states will be reduced that the trapped electrons can be thermally emitted into the conductive states, forming a FP emission current (I_{FP}). The *I-V* relationship can be described by[16]

$$I_{FP} \propto F \exp\left[\frac{-q(\varphi_B - \beta\sqrt{F})}{kT}\right], \tag{6}$$

where F is the average electric field strength, $q\varphi_B$ is the zero-field emission barrier height, and $\beta = \sqrt{q/\pi\varepsilon\varepsilon_0}$ is the FP emission coefficient. Physically, when the electric filed becomes large enough that a triangular barrier is formed, the FN tunneling process can take place. The *I-V* characteristics is given as[17]

$$I_{FN} \propto F^2 \exp\left(-\frac{B}{F}\right), \tag{7a}$$

$$B = \frac{8\pi\sqrt{2m_n^*(q\phi_{eff})^3}}{3qh}, \tag{7b}$$

where m_n* is the effective mass of electron, h is Planck's constant, and $q\phi_{eff}$ is the effective tunneling barrier height. Figure 7 shows the fitting results of the reverse current characteristics at 300 K and 500 K, respectively. The experimental data agree well with the FP emission model at low bias; while at high bias the current is governed by the FN tunneling mechanism. The critical voltage for FN tunneling is about 5 V, and the corresponding electric field is determined ~6 MV/cm based on the capacitance characteristics of the device. Figure 8 illustrates the schematic reverse current transport processes: (1) at low fields, the interface electrons trapped at the Fermi level between the metal and the semiconductor layers can be readily emitted to the continuous electrical states associated with linear dislocations with a reduced barrier height (Fig. 8(a)); (2) at higher fields the current begins to flow by means of a FN tunneling process due to the formation of a triangular barrier (Fig. 8(b)).

Rearranging Eq. (6), we have

$$\ln(I_{FP}/F) \propto \frac{q\beta}{kT}\sqrt{F} - c(T), \tag{8a}$$

$$c(T) = \frac{q\varphi_B}{kT}. \tag{8b}$$

The above equations clearly predict that if the leakage current is dominated by FP emission, both of the $\ln(I_{FP}/F)$ versus $F^{0.5}$ and c(T) versus $1/kT$ plots should follow a linear dependence but with different slope. As shown in Fig. 9(a), the experimental data can be well fitted with Eq. (8a), and the $q\varphi_B$ value is determined 0.62 eV, which is quite close to the result recently reported by Turuvekere *et al.*,[18]

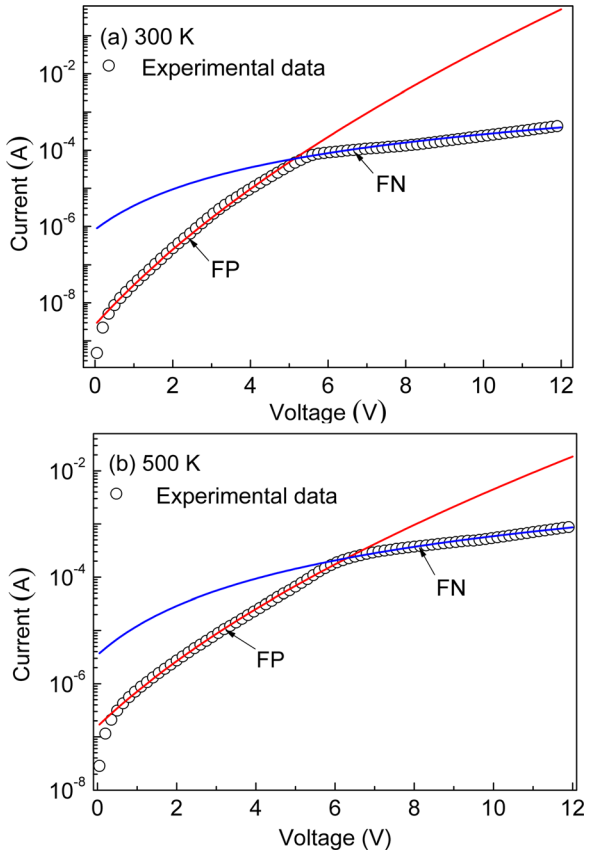

FIG. 7. Fitting results of the reverse *I-V* characteristics of InAlN/GaN Schottky diode measured at 300 K (a) and 500 K (b), respectively.

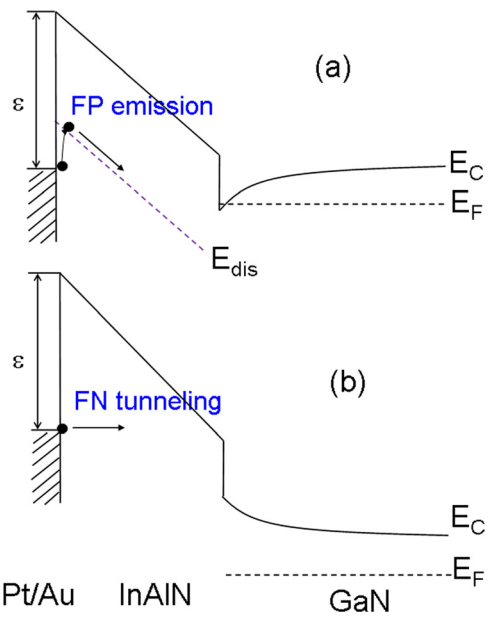

FIG. 8. Schematic diagram of the reverse current transport mechanism of InAlN/GaN Schottky diode: (a) FP emission; (b) FN tunneling. The solid dots represent electrons in GaN.

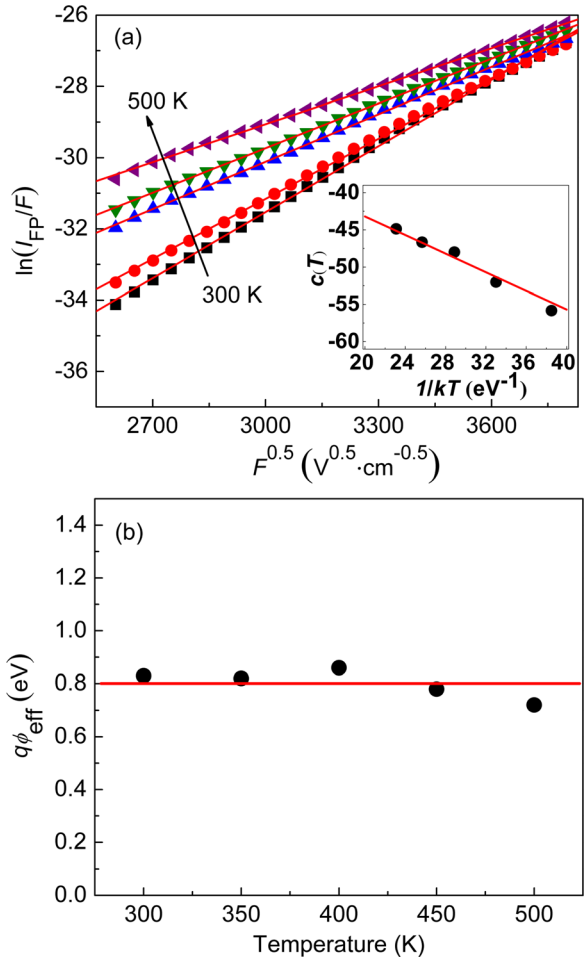

FIG. 9. (a) Linear relation between $\ln(I_{FP}/F)$ and $F^{0.5}$ at different temperatures, with the $c(T)$-q/kT relation plotted in the inset; (b) temperature dependence of the effective FN tunneling barrier height.

suggesting that the energy position of the conductive states is about 0.62 eV above the metal Fermi level at zero field. The effective tunneling barrier height $q\phi_{eff}$ at different temperatures is determined 0.80 eV by fitting the FN tunneling current (Fig. 9(b)), which is not sensitive to temperature, confirming the FN tunneling mechanism. Note that, $q\phi_{eff}$ is about 0.18 eV larger than $q\varphi_B$, indicating that the continuous energy states associated with the linear dislocations should locate at 0.18 eV below the conduction band edge.

IV. CONCLUSIONS

The forward and reverse current transport mechanisms in lattice-matched Pt/Au-InAlN/GaN Schottky diodes are investigated by fitting experimental *T*-*I*-*V* characteristics. The results indicate that the traditional TE model can only describe the forward-high-bias *I*-*V* characteristics, while the forward-low-bias current is mainly attributed to the TAT mechanism. The reverse leakage current under low electric fields (<6 MV/cm) is mainly carried by the FP emission electrons, while at higher fields the FN tunneling current dominates. The calculated effective defect density of about $5.5 \times 10^9\,cm^{-2}$ and the FP emission barrier height of 0.62 eV suggest that structural defects, such as N vacancies and threading dislocations, have an important influence on electrical properties of this device.

ACKNOWLEDGMENTS

This work was supported by China Postdoctoral Science Foundation (2013M540437), Natural Science Foundation of Jiangsu Province (BK2012110), Fundamental Research Funds for the Central Universities (JUSRP51323B and JUDCF13038), the Graduate Student Innovation Program for University of Jiangsu Province (CXLX13-740), and the Summit of the Six Top Talents Program of Jiangsu Province (DZXX-053).

[1]S. Corekci, M. K. Oztuurk, B. Akaoglu, M. Cakmak, S. Ozcelik, and E. Ozbay, J Appl. Phys. **101**, 123502 (2007).
[2]A. Y. Polyakov, N. B. Smirnov, A. V. Govorkov, A. V. Markov, T. G. Yogova, A. M. Dabiran, A. M. Wowchak, B. Cui, A. V. Osinsky, P. P. Chow, S. J. Pearton, K. D. Scherbatchev, and V. T. Bublik, J Appl. Phys. **104**, 053702 (2008).
[3]M. Meneghini, A. Stocco, M. Bertin, D. Marcon, and A. Chini, Appl. Phys. Lett. **102**, 163501 (2013).
[4]J. Ren, D. W. Yan, and X. F. Gu, Acta Phys. Sin. **62**, 157202 (2013).
[5]J. Joh and J. A. del Alamo, IEEE Electron Device Lett. **29**, 287 (2008).
[6]J. Kuzmik, IEEE Electron Device Lett. **22**, 510 (2001).
[7]E. Arslan, I. N. S. Alt, S. Ozcelik, and E. Ozbay, J. Appl. Phys. **105**, 23705 (2009).
[8]D. Donoval, A. Chvala, R. Sramaty, J. Kovac, and P. Kordos, Appl. Phys. Lett. **96**, 223501 (2010).
[9]D. Donoval, M. Barus, and M. Zdimal, Solid-State Electron. **34**, 1365 (1991).
[10]S. Alialy, H. U. S. Tecimer, and H. Uslu, J. Nanomed. Nanotechnol. **4**, 167 (2013).
[11]D. W. Yan, H. Lu, D. S. Cao, D. J. Chen, R. Zhang, and Y. D. Zheng, Appl. Phys. Lett. **97**, 153503 (2010).
[12]H. Angerer, D. Brunner, F. Freudenberg, O. Ambacher, M. Stutzmann, R. Hopler, T. Metzger, E. Born, G. Dollinger, A. Bergaier, S. Karsch, and H. J. Korner, Appl. Phys. Lett. **71**, 1504 (1997).
[13]B. K. Li, M. J. Wang, K. J. Chen, and J. N. Wang, Appl. Phys. Lett. **95**, 232111 (2009).
[14]K. Saarinen and P. Seppala, Appl. Phys. Lett. **22**, 3253 (1998).
[15]D. W. Yan, H. Lu, D. J. Chen, R. Zhang, and Y. D. Zheng, Appl. Phys. Lett. **96**, 083504 (2010).
[16]E. Arslan, S. Butun, and E. Ozbay, Appl. Phys. Lett. **94**, 142106 (2009).
[17]O. Briere, K. Brrla, A. Hamaui, and G. Ghibaudo, Solid-State Electron. **41**, 987 (1997).
[18]S. Turuvekere, N. Karumuri, A. A. Rahman, A. Bhattacharya, A. DasGupta, and N. DasGupta, IEEE Trans. Electron Devices **60**, 3157 (2013).